

PAPER • OPEN ACCESS

Mechanical Degradation Model of Porous Fe Scaffold: Simulation Approach

To cite this article: Akbar Teguh Prakoso *et al* 2020 *J. Phys.: Conf. Ser.* **1500** 012023

Recent citations

- [Effects of conform, non-conform, and hybrid conformity toward stress distribution at the glenoid implant and cement: A finite element study](#)
Abdul Hadi Abdul Wahab *et al*

View the [article online](#) for updates and enhancements.

A promotional banner for the 240th ECS Meeting. The banner features the ECS logo on the left, followed by the text '240th ECS Meeting' in large blue font, 'Digital Meeting, Oct 10-14, 2021' in smaller blue font, 'We are going fully digital!' in green font, 'Attendees register for free!' in black font, and 'REGISTER NOW' in orange font. On the right side of the banner is a photograph of a diverse group of people in a professional setting, with a man in a white shirt and tie clapping and smiling.

ECS **240th ECS Meeting**
Digital Meeting, Oct 10-14, 2021
We are going fully digital!
Attendees register for free!
REGISTER NOW

Mechanical Degradation Model of Porous Fe Scaffold: Simulation Approach

Akbar Teguh Prakoso¹, Achmad Rendiko Ichsan¹, Ardiyansyah Syahrom^{2,3}, Amir Putra Md Saad^{2,3}, Abdul Hadi Abdul Wahab⁴, M. A. Sulong^{2,3}, F.A. Mohd Ghazali², Hasan Basri^{1*}

¹Departement of Mechanical Engineering, Faculty of Engineering, Universitas Sriwijaya, Kabupaten Ogan Ilir, Palembang, Sumatera Selatan, Indonesia.

²Applied Mechanics and Design, School of Mechanical Engineering, Faculty of Engineering, Universiti Teknologi Malaysia (UTM), 81410 Johor Bahru, Malaysia.

³Medical Devices and Technology Centre (MEDITEC), Institute of Human Centred and Engineering (iHumEn), Universiti Teknologi Malaysia (UTM), 81310 Johor Bahru, Malaysia.

⁴Faculty of Biosciences and Medical Engineering, Medical Devices and Technology Group, Universiti Teknologi Malaysia, Johor, Malaysia.

* Email: hasan_basri@unsri.ac.id

Abstract. This paper proposes a simple degradation model that estimates morphological changes in pure iron scaffolding due to surface erosion. The main contribution of this work is to estimate the degradation of porous pure iron scaffolding and analyze the impact of morphological changes on mechanical properties. In this study, the pure iron scaffolding model was designed in CAD software with 3 different porosity such as 30%, 41%, and 55% respectively. The geometry images of CAD models with a resolution of 3316 x 5530 pixels are captured layer by layer with a thickness of 0.02 mm. The purpose of this method is to replace the function of the μ -CT scanning technique. Two-dimensional morphological erosion is applied to reduce the number of pixels of the image model. This erosion process is adjusted iteratively with increasing number of pixels to erode the image model until the volume of the scaffold after reconstruction matches the volume of the model undergoing mathematical calculations. Their changes in the volume of scaffold geometry and degradation of mechanical properties were evaluated using finite element analysis. This study found that mechanical properties such as elastic modulus and yield strength decreased systematically during the 19 week degradation period. In addition, deformation analysis is performed on models based on finite element analysis.

Keywords: Scaffold, pure iron, degradation, morphology, surface erosion, mechanical properties, finite element analysis.

1. Introduction

Bone tissue engineering scaffolds made of biodegradable material for bone replacement has been shown to be a promising scaffold for triggering bone tissue regeneration and provide sufficient support until completing the tissue healing process. There are known biodegradable materials based on polymers, ceramics, and bioactive glass for orthopedic purposes; however, their mechanical properties are not suitable for bone load-bearing implants applications, in contrast to metallic biomaterials [1–4]. Three



metal biomaterials, based on Iron (Fe), Zinc (Zn) and Magnesium (Mg), have been studied over the past decade and are thought to be possible materials for the production of biodegradable, load-bearing orthopedic implants [4–9]. A majority of the available investigations have been performed using magnesium-based biomaterials because magnesium is potential to degrade in vivo without causing toxicological problems and its mechanical properties in the range of human bone [10]. However, Mg-based biodegradable materials have high corrosion rates and that is a major limitation which results in poor mechanical integrity and the fact that the problem of hydrogen evolution drastically complicates the healing process [6]. In contrast, the degradation rates of Zinc and its alloys are suitable for applications that can biodegrade, but the mechanical properties and high density of these materials limit their applications [10]. Compared with Zinc and Magnesium, Iron possesses significantly higher value of mechanical strength. Elastic modulus of Fe too high as compared human bone [11], but it can be decreased by creating porous structure on the material. In addition, the degradation rate of metallic iron in body fluids is significantly lower than zinc and magnesium and the corrosion product is not connected with hydrogen evolution [12]. Furthermore, in vitro and in vivo test have been performed in previous investigation and the results shows that iron based materials suitable materials for biodegradable load-bearing implant [9, 13–15].

Mechanical degradation of pure iron scaffold has been investigated in previous study by experimental procedures [16–18]. However, this method is time-consuming and high cost with limited applicability for extensive studies. These drawbacks can be overcome by the additional use of mathematical and numerical models. Previous researchers [19,20] presented mathematical models to analyze biodegradation of biopolymer. Adachi et al. [21] has been successfully develop a polymeric biomaterials degradation simulation based on voxel finite element to degrade surface of the scaffold and remodeling a new bone in the same time frame. The simulation method is promising for optimization of porous scaffold microstructure design. However, the method process is very complex despite using simple rate equations for new bone formation and degradation of scaffold being used. Sanz-Herrera and Boccaccini [22] presented a novel theoretical model for the analysis and simulation degradation and bioactivity of bioactive glass through Voxel-FEM method. Another investigation, degradation simulation of titanium based on phenomenological method to predict the change of complex geometry of scaffold due to surface erosion at different stages [23]. To the best of our knowledge, the degradation simulation of pure iron and impact its morphological parameters to the mechanical properties has not presented yet.

The focus of this study is the simulation of predicted scaffold geometry changes due to degradation and its effect on mechanical properties. For this purpose, raw image data from the pure iron scaffold model is processed and partially degraded geometry is calculated. Scaffolding geometry after degradation is obtained and then used to conduct finite element analysis to assess degradation of mechanical properties such as Young's modulus and yield strength. This method provides a means to assess the macro architecture of bone tissue and bone scaffolding, before and after implantation. The mechanical integrity of bone scaffolding can be anticipated, where morphological changes as structural support are analyzed. In addition, the mechanical strength of bone scaffolding is largely determined by its degradation behavior, especially to the completion of the healing process of bone tissue. Finally, this method provides the basic features of the proposed framework for the optimal design of a porous scaffolding macro structure taking into account its degradation behavior.

2. Material and Method

2.1. 3D-Model Preparation and Characterization

Three-dimensional of porous pure iron models are generated using a computer-aided design (CAD) software into cuboid-shaped with model measuring 5 x 5 x 3 mm. The percentage porosity of the model

is varied and the pore size is 800 μm demonstrated in Figure 1. The morphological parameters of the model calculated using software commands are presented in Table 1.

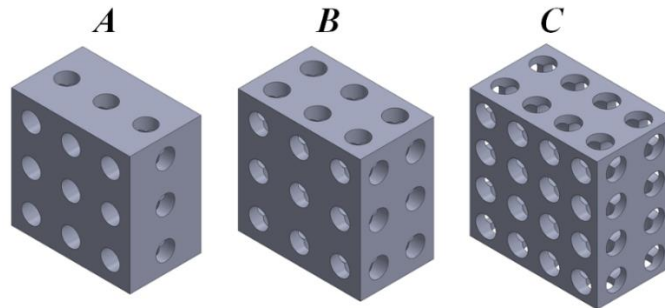


Figure 1. Three different morphologies of porous model: A) 30%, B) 41%, C) 55% porosity [24]

Table 1. The morphological parameters detail of the CAD models

Model	Porosity, p (%)	Surface Area (mm^2)	Volume (mm^3)	Height (mm)	Mass (mg)
A	30 %	189.30	52.87	5	416.08
B	41%	209.81	45.57	5	350.76
C	55%	225.75	33.83	5	266.24

*density of pure iron $\rho = 7.87 \text{ g/cm}^3$

2.2. Degradation rate of pure iron

Biodegradation rate of pure iron demonstrated in Figure 2. The degradation rate of pure iron can be expressed using logarithmic regression functions. This function scales the degradation rate of pure iron [25] according to the time of immersion [24].

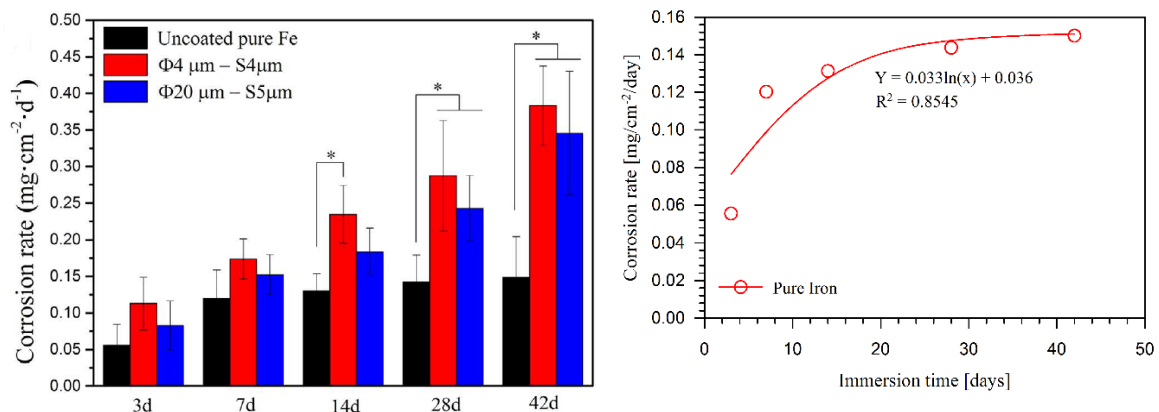


Figure 2. Degradation rate of pure uncoated pure Fe is taken from Huang et al. [25]

The logarithmic regression model equation that shows the correlation between the degradation time and the degradation rate can be represented as follows:

$$\text{Degradation rate} = 0.033 \ln(\text{degradation time}) + 0.036 \quad (1)$$

Using logarithmic regression model, W_f model based on degradation has been obtained [26].

$$\Delta W_m = \frac{W_o - W_f}{At} \quad (2)$$

$$W_f = W_o - (\Delta W_m * At) \quad (3)$$

Where ΔW_m is degradation rate value, W_f and W_o are weight model after and before degradation respectively, A is surface area in contact with SBF is similar to the exposed surface area of the model in mm^2 , and t is time of exposure in days. Finally, the volume after degradation was calculated using equation as follow:

$$V_f = \frac{W_f}{\rho} \quad (4)$$

2.3. 3D-Model Preparation and Characterization

Two basic mechanisms of degradation are usually distinguished. Surface erosion and bulk degradation. For Fe-based biodegradable alloy, the ideal degradation process under immersion in Hank's solution has been addressed in previous research [27]. Theoretically, localized degradation of pure iron is more likely to occur in a high chloride ion concentration solution and in crevices. In addition, a non-uniform stress distribution at different points along a bone scaffold is a potential factor influencing the induction of localized degradation. To enhance general degradation in the living tissue, two kinds of improvements might be helpful, as shown in the idealized degradation process in Figure 3. A Pits should be formed as much as possible during formation and propagation stages. As the time goes on and the pits grow, they will become connected, forming and degraded surface. General degradation can be achieved as all metals beneath are in the same degradation product covered condition. Decreasing the pitting potential or introducing a widespread secondary phase intermetallic network is possible way to realize this ideal degradation process. Furthermore, in section B, the pits grow in the horizontal direction. It is hard pits to grow in this way because of the self-catalytic mechanism of iron degradation. The inhibition of localized acidification and increasing the degradation potential of the degradation products could be trying to solve this problem.

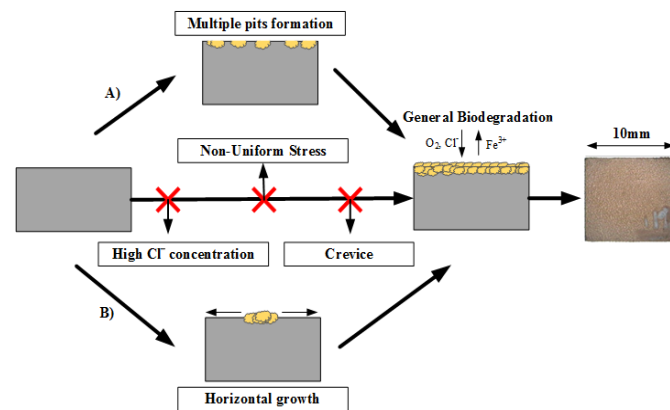


Figure 3. Schematic diagram for ideal degradation process Fe-based biodegradable alloys in Hank's solution [27]

In order to develop a degradation simulation of porous iron scaffolds, we assumed the material undergo ideal degradation process, which is manifested in the gradual thinning of the scaffolds without localized degradation. This investigation considers surface erosion, which is better suited to describe the degradation behaviour of pure iron scaffolds. The schematic diagram process to obtain 3D degradation model of porous iron scaffold is illustrated step-by-step in Figure 4. The geometric images of CAD models with a resolution of 3316 x 5530 pixels are captured layer by layer with a thickness of 0.02 mm using the software command. The purpose of this method is to replace a function of the μCT scanning technique. The μCT scanning technique has been used in tissue engineering to aim the scaffold evaluation /tissue integration, tissue formation and scaffold degradation [28]. After that, the images are

transformed into binary form or simply black and white voxel using *image J* software. Segmentation or thresholding procedure is conducted by using MIMICS (Materialise, Leuven, Belgium) to select the region of interest (ROI) area. Furthermore, 2-D morphological erosion command is applied to decrease pixel number of the images model. This erosion process is iteratively adjusted with increasing number of pixels to erode the images model until the volume scaffold after reconstruction V_{dm} matches with the model volume V_{mc} which underwent the mathematical calculation. In this work, the 3D model degradation simulation was set for 28, 68, 90, and 135 days respectively.

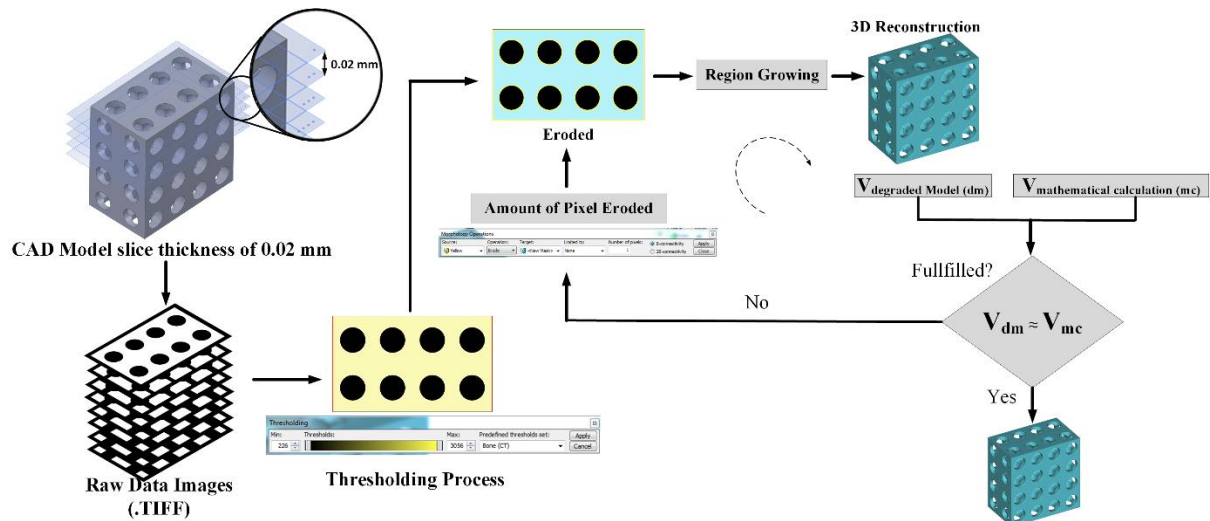


Figure 4. Schematic diagram simulation process to obtain degradation model of porous iron scaffold

Finally, the 3D reconstruction model is obtained with the 3D mask calculate software command and the tabulation results of degradation simulation can be shown in Table 2.

Table 2. The morphology indices of pure iron bone scaffold before and after degradation simulation

Model	Time, (days)	BV	TV	BV/TV	Porosity (%)
A	0	52.5521		0.70069	29.93053
	28	51.689341		0.68919	31.08087
	68	50.05806	75	0.66744	33.25592
	90	48.97895		0.65305	34.69473
	135	46.31015		0.61746	38.25313
B	0	44.43369		0.59244	40.75508
	28	43.38259		0.57843	42.15654
	68	41.43564	75	0.55247	44.75248
	90	40.14729		0.53529	46.47028
	135	37.59306		0.50124	49.87592
C	0	33.77488		0.45033	54.96682
	28	32.77892		0.43705	56.29477
	68	30.31739	75	0.40423	59.57681
	90	29.10741		0.38809	61.19012
	135	26.14338		0.34857	65.14216

2.4. Finite Element Simulation

Finite element simulation is a numerical model to analyse the mechanical characterization of porous iron scaffold using a virtual model. By using this approach, modulus of elasticity, yield strength (σ_{ys}), stress distribution, and deformation of the sample can be obtained.

2.4.1. Material and Model. In order to calculate the structure properties of the porous scaffold model using numerical simulation, the mechanical properties of solid pure iron are used in this scope of the investigation. Mechanical properties data of commercially available pure iron rod with 99.8% purity (made by Goodfellow Inc, Cambridge, UK) as shown in Table 3 [30].

Table 3. The mechanical properties of Fe (made of Goodfellow Inc, Cambridge, UK) [30]

Density ρ (g/cm ³)	Elastic Modulus (GPa)	Poisson's ratio	Yield Strength σ_{ys} (MPa)
7.87	200	0.3	150

2.4.2. Boundary Condition and Evaluation. The reconstruction of 3D model scaffold before and after degradation were exported to finite element analysis using MSC.Marc® integrated by a user subroutine. Finite element analysis in the present investigation to imitate quasi-static compression in order to determine the structural properties of the porous iron. The boundary conditions of all models demonstrated in Figure 5. A time-dependent displacement boundary condition was defined on the top surface to simulate the moving load cell of an experimental test rig. In addition, a fix-displacement boundary condition in the y-direction is assigned the opposite surface in its normal direction but x and y-direction move freely inside the x-y plane. The model is fixed in the y-direction at the bottom and a uniform compressive strain limit $\epsilon = 0.3$ is applied to the top surface of the model to mimic in vitro experimental testing conditions.

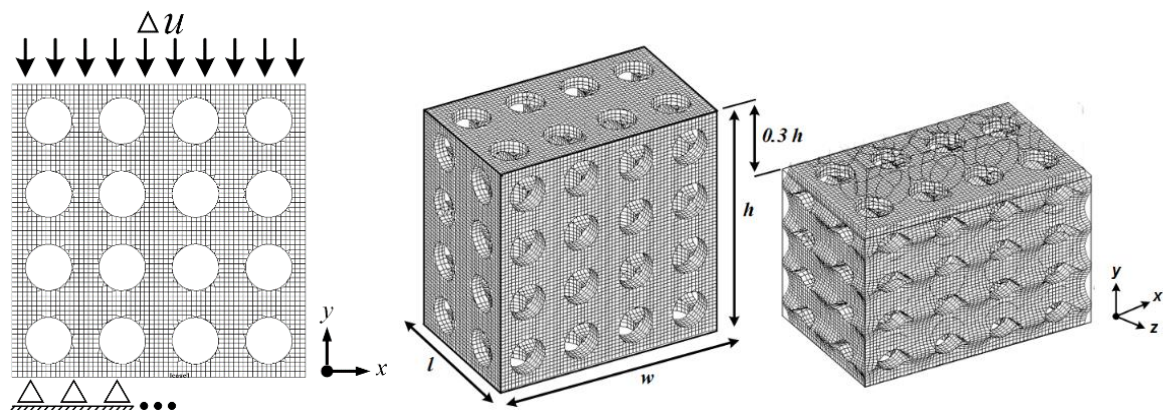


Figure 5. Schematic illustration of boundary conditions applied to the numerical model

As validation requirement, the boundary condition is valid according when the experimental and simulation line on stress-strain curve is coincide the each other. Meanwhile as shown in Figure 6, the stress-strain curve of solid pure iron under compressive load has a good agreement between simulation and experimental data on the slope of the elastic region. As a result, this boundary condition is applied for simulate the mechanical properties of porous scaffold model before and after degradation.

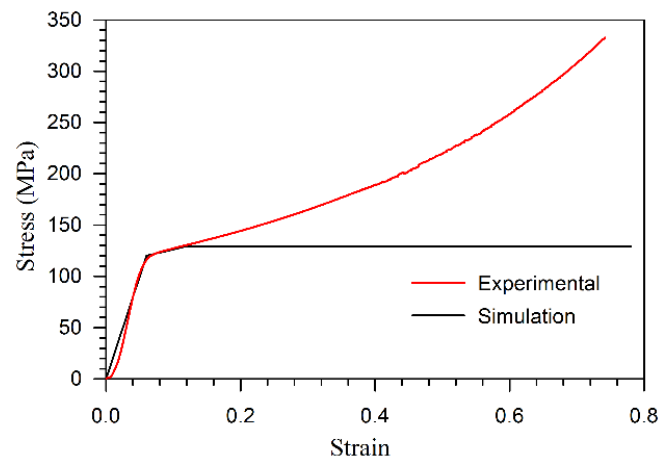


Figure 6. Comparison of Stress-Strain curve between the finite element simulation and the experimental of bulk pure iron specimen

3. Results and Discussion

3.1. The stress-strain curve

The quasi-static compressive stress-strain curve of porous pure iron with different porosities have been obtained from numerical simulation which is illustrated in Figure 7. The stress strain curves are represented by different line color types namely red, blue, magenta, cyan, and black for 0, 28, 68, 90, and 135 days respectively. It can be observed that the stresses gradually decrease as the degradation time increase due to increasing porosity caused by surface erosion. This phenomenon may arise from the fact that the porosity, p increases from A ($p = 29.93\%$) – C ($p = 54.96\%$). The linear correlation between mechanical properties and porosity is widely documented in the literature for metallic foams and porous biomaterials [30][31].

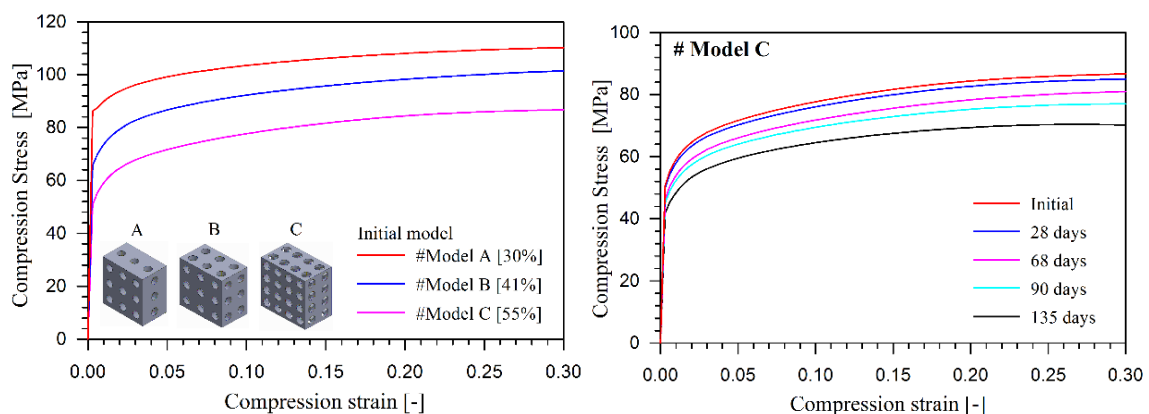


Figure 7. Stress-strain curves from finite element simulations.

Using stress-strain data in Figure 7, elastic modulus E , and yield strength $\sigma_{0.2}$ can be determined. The summary of mechanical properties of all models are illustrated in Figure 8. In general, all mechanical properties are gradually decrease in similar pattern. The result shows that the mechanical response appears to weaken with increasing the degradation time in simulation before-after degradation. A logical explanation of this behaviour is may due to eroded struts and thin walls, which deteriorate the mechanical integrity of the scaffolds as demonstrated in Figure 10. In yield strength, the values of the initial scaffolds are in the range of 54.96 – 87.74 MPa. The maximum value belongs to model A (87.74

MPa) and the minimum value corresponds to model C (54.967 MPa). In elastic modulus, the values of the initial scaffold are in the range 28.7, 21.8, and 16.9 GPa for model A, B and C respectively. Furthermore, the ordered and controllable porous structure techniques for elastic modulus of the porous FE scaffold can be controllable precisely by adjusting the porosity and arranging the pores [33,34]. In this study, the elastic modulus of porous Fe scaffolds has been similar with the cancellous bone structure based on different anatomical site in previous investigation. Such as, human cancellous bone in proximal tibia (23.6 ± 3.34 GPa), greater trochanter (24.4 ± 2.0 GPa), for femoral neck (18 ± 2.8 GPa) [35], for human femur (17.5 ± 1.12 GPa), distal femur (18.1 ± 1.7 GPa) [36], femoral head (21.8 ± 2.9 GPa), femur trochanter (21.3 ± 2.1 GPa) [37] and (19.4 ± 2.3 GPa) for tibia/vertebrae [38]. This information is crucial in order to apply the bone scaffold for load bearing purposes. In fact, one possible implant loosening mechanism that followed to stress shielding effect, poor osteointegration and bone resorption is incompatibility between elastic modulus of bone scaffold and cancellous bone [39]. In additional, the mechanical properties reduced after model degrades for 28, 68, 90, and 135 days respectively. It can be concluded that porous pure iron scaffolds begin to lose their structural integrity proportional to the increasing degradation period.

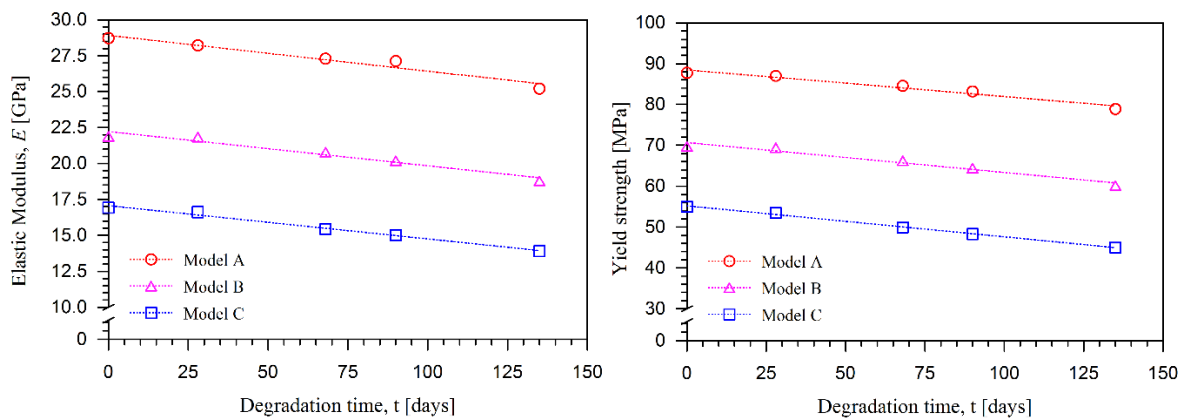


Figure 8. Elastic modulus and yield strength determined by simulation

Furthermore, the effect of morphological changes on the elastic modulus of porous scaffold had strong correlation as demonstrated in Figure 9. The alteration of porous scaffold due to degradation has caused large changes to the specimen with a higher percentage of porosity [40]. Consequently, the degradation has weakened the struts of the structure and it could be reduced the stiffness of scaffold that indicated by the decrease of elastic modulus (see Figure 10). Unfortunately, degradation simulation was assumed ideal degradation process without localized degradation caused by high Cl^- concentration, non-uniform stress and crevice. This degradation phenomenon is impossible to occur when scaffold implanted into bone tissue environment with different flow rate in bone marrow [41].

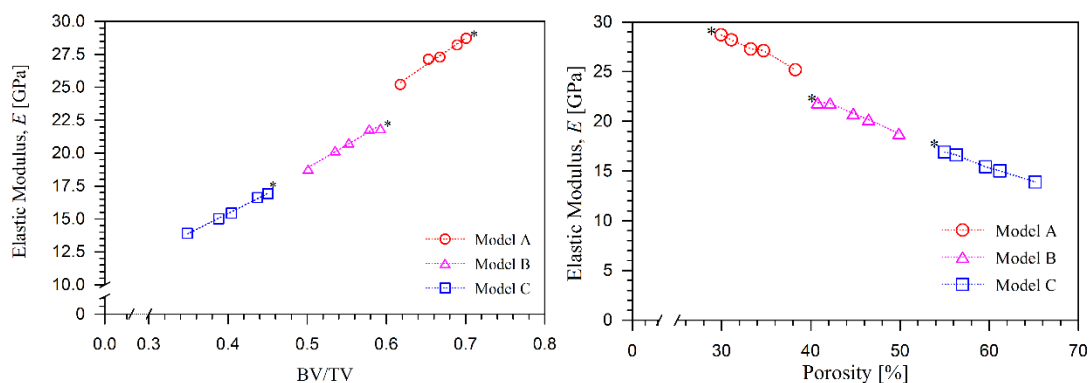


Figure 9. the effect of morphological changes (BV/TV & porosity) on the elastic modulus of porous scaffold

The fracture characteristic of porous scaffold before and after degradation can be shown in Figure 10 denoted by dash line and high principal elastic strain. The characteristic of fracture is similar to actual cancellous bone indicated by global fracture [42], this could represent the damage behavior of the scaffold once implanted to prevent different directional stress effects.

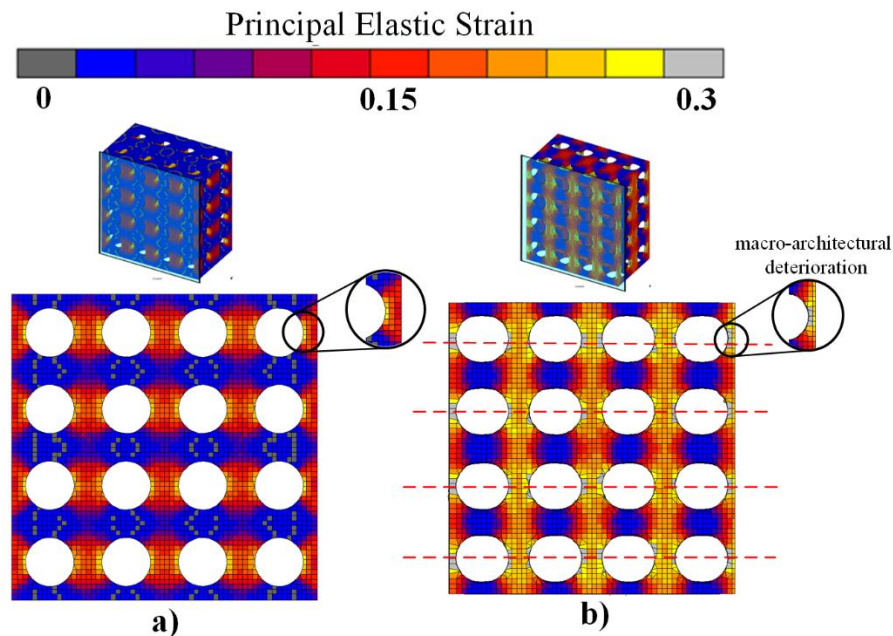


Figure 10. Contour plots of the fracture pattern a) before and b) after degradation simulation.

4. Conclusion

In this study, the mechanism of degradation has been simulated using phenomenological methods to predict surface erosion at various stages due to immersion in body fluids. Mechanical porous degradation of Fe has been discussed in this paper using numerical analysis based on finite element analysis. General mechanical properties (elastic modulus and yield strength) are reduced by $\sim 19\%$ from the initial state when the sample reaches a 135 days degradation period. The results showed that the mechanical properties and morphological parameters had a good correlation with $R^2 = 0.98$. Finally, a detailed fracture characteristic analysis is performed on the model based on finite element analysis. The characteristics of a fracture are similar to the actual cancellous bone shown by global fractures.

Acknowledgment

This work was funded by Universitas Sriwijaya Grant entitled “One-to-One Research Matching Grant Universitas Sriwijaya and Universiti Teknologi Malaysia. The authors would like to thank the Research Management Centre (LPPM), Universitas Sriwijaya, for managing the project.

References

- [1] S. Wu, X. Liu, K. W. K. Yeung, C. Liu, and X. Yang, “Biomimetic porous scaffolds for bone tissue engineering,” *Mater. Sci. Eng. R Reports*, vol. 80, no. 1, pp. 1–36, 2014.
- [2] D. W. Huttmacher, “Scaffolds in tissue engineering bone and cartilage,” in *The Biomaterials: Silver Jubilee Compendium*, 2006.
- [3] K. Alvarez and H. Nakajima, “Metallic scaffolds for bone regeneration,” *Materials (Basel)*, 2009.
- [4] H. Kitabata, R. Waksman, and B. Warnack, “Bioresorbable metal scaffold for cardiovascular application: Current knowledge and future perspectives,” *Cardiovascular Revascularization Medicine*. 2014.

- [5] M. P. Staiger, A. M. Pietak, J. Huadmai, and G. Dias, "Magnesium and its alloys as orthopedic biomaterials: A review," *Biomaterials*, 2006.
- [6] H. Hermawan, D. Dubé, and D. Mantovani, "Degradable metallic biomaterials: Design and development of Fe-Mn alloys for stents," *J. Biomed. Mater. Res. - Part A*, 2010.
- [7] F. Witte *et al.*, "Biodegradable magnesium-hydroxyapatite metal matrix composites," *Biomaterials*, 2007.
- [8] H. Hermawan and D. Mantovani, "Process of prototyping coronary stents from biodegradable Fe-Mn alloys," *Acta Biomater.*, 2013.
- [9] M. Moravej and D. Mantovani, "Biodegradable metals for cardiovascular stent application: Interests and new opportunities," *International Journal of Molecular Sciences*, 2011.
- [10] Y. F. Zheng, X. N. Gu, and F. Witte, "Biodegradable metals," *Mater. Sci. Eng. R Reports*, vol. 77, pp. 1–34, 2014.
- [11] M. Peuster *et al.*, "A novel approach to temporary stenting: Degradable cardiovascular stents produced from corrodible metal - Results 6-18 months after implantation into New Zealand white rabbits," *Heart*, 2001.
- [12] J. Cheng, B. Liu, Y. H. Wu, and Y. F. Zheng, "Comparative invitro study on pure metals (Fe, Mn, Mg, Zn and W) as biodegradable metals," *J. Mater. Sci. Technol.*, vol. 29, no. 7, pp. 619–627, 2013.
- [13] H. Hermawan, A. Purnama, D. Dube, J. Couet, and D. Mantovani, "Fe-Mn alloys for metallic biodegradable stents: Degradation and cell viability studies," *Acta Biomater.*, 2010.
- [14] B. Wegener *et al.*, "Microstructure, cytotoxicity and corrosion of powder-metallurgical iron alloys for biodegradable bone replacement materials," in *Materials Science and Engineering B: Solid-State Materials for Advanced Technology*, 2011.
- [15] M. Peuster, C. Hesse, T. Schloo, C. Fink, P. Beerbaum, and C. von Schnakenburg, "Long-term biocompatibility of a corrodible peripheral iron stent in the porcine descending aorta," *Biomaterials*, 2006.
- [16] P. Sharma and P. M. Pandey, "Corrosion behaviour of the porous iron scaffold in simulated body fluid for biodegradable implant application," *Mater. Sci. Eng. C*, 2019.
- [17] R. Oriňáková *et al.*, "Iron based degradable foam structures for potential orthopedic applications," *Int. J. Electrochem. Sci.*, vol. 8, no. 12, pp. 12451–12465, 2013.
- [18] P. Sharma and P. M. Pandey, "A novel manufacturing route for the fabrication of topologically-ordered open-cell porous iron scaffold," *Mater. Lett.*, 2018.
- [19] X. Han and J. Pan, "A model for simultaneous crystallisation and biodegradation of biodegradable polymers," *Biomaterials*, 2009.
- [20] Y. Wang, J. Pan, X. Han, C. Sinka, and L. Ding, "A phenomenological model for the degradation of biodegradable polymers," *Biomaterials*, 2008.
- [21] T. Adachi, Y. Osako, M. Tanaka, M. Hojo, and S. J. Hollister, "Framework for optimal design of porous scaffold microstructure by computational simulation of bone regeneration," *Biomaterials*, vol. 27, no. 21, pp. 3964–3972, 2006.
- [22] J. A. Sanz-Herrera and A. R. Boccaccini, "Modelling bioactivity and degradation of bioactive glass based tissue engineering scaffolds," *Int. J. Solids Struct.*, 2011.
- [23] M. A. Sulong, I. V. Belova, A. R. Boccaccini, G. E. Murch, and T. Fiedler, "A model of the mechanical degradation of foam replicated scaffolds," *J. Mater. Sci.*, vol. 51, no. 8, pp. 3824–3835, 2016.
- [24] A. T. Prakoso *et al.*, "A comparison of degradation rate bone scaffold morphology between computer simulation and experimental approach," *Malaysian J. Fundam. Appl. Sci. Spec. Issue Med. Device Technol.*, no. December, pp. 529–532, 2017.
- [25] T. Huang and Y. Zheng, "Uniform and accelerated degradation of pure iron patterned by Pt disc arrays," *Sci. Rep.*, vol. 6, no. April, pp. 1–11, 2016.
- [26] A. P. Md Saad *et al.*, "Dynamic degradation of porous magnesium under a simulated environment of human cancellous bone," *Corros. Sci.*, vol. 112, pp. 495–506, 2016.

- [27] B. Liu and Y. F. Zheng, "Effects of alloying elements (Mn, Co, Al, W, Sn, B, C and S) on biodegradability and in vitro biocompatibility of pure iron," *Acta Biomater.*, vol. 7, no. 3, pp. 1407–1420, 2011.
- [28] R. Cancedda, "Kinetics of In Vivo Bone Deposition by Bone Marrow Stromal Cells Within a Resorbable Porous Calcium Phosphate Scaffold: An X-Ray Computed Microtomography Study," *Biotechnol. Bioeng.*, vol. 98, No. 1, no. Ii, pp. 271–281, 2007.
- [29] O. Caty, E. Maire, S. Youssef, and R. Bouchet, "Modeling the properties of closed-cell cellular materials from tomography images using finite shell elements," *Acta Mater.*, vol. 56, no. 19, pp. 5524–5534, 2008.
- [30] D. R. and J. R. P. D. Hendra Hermawan, *Metals for Biomedical Application*. InTech, 2011.
- [31] K. Rezwan, Q. Z. Chen, J. J. Blaker, and A. R. Boccaccini, "Biodegradable and bioactive porous polymer/inorganic composite scaffolds for bone tissue engineering," *Biomaterials*, vol. 27, no. 18, pp. 3413–3431, 2006.
- [32] F. G. Torres, S. N. Nazhat, S. H. Sheikh Md Fadzullah, V. Maquet, and A. R. Boccaccini, "Mechanical properties and bioactivity of porous PLGA/TiO₂ nanoparticle-filled composites for tissue engineering scaffolds," *Compos. Sci. Technol.*, vol. 67, no. 6, pp. 1139–1147, 2007.
- [33] S. Bose, M. Roy, and A. Bandyopadhyay, "Recent advances in bone tissue engineering scaffolds," *Trends Biotechnol.*, vol. 30, no. 10, pp. 546–554, 2012.
- [34] G. Jiang and G. He, "A new approach to the fabrication of porous magnesium with well-controlled 3D pore structure for orthopedic applications," *Mater. Sci. Eng. C*, 2014.
- [35] E. F. Morgan, H. H. Bayraktar, and T. M. Keaveny, "Trabecular bone modulus-density relationships depend on anatomic site," *J. Biomech.*, 2003.
- [36] C. H. Turner, J. Rho, Y. Takano, T. Y. Tsui, and G. M. Pharr, "The elastic properties of trabecular and cortical bone tissues are similar: Results from two microscopic measurement techniques," *J. Biomech.*, 1999.
- [37] S. Dendorfer, H. J. Maier, and J. Hammer, "Fatigue damage in cancellous bone: An experimental approach from continuum to micro scale," *J. Mech. Behav. Biomed. Mater.*, vol. 2, no. 1, pp. 113–119, 2009.
- [38] J. Y. Rho, T. Y. Tsui, and G. M. Pharr, "Elastic properties of human cortical and trabecular lamellar bone measured by nanoindentation," *Biomaterials*, 1997.
- [39] L. Shi *et al.*, "The Improved Biological Performance of a Novel Low Elastic Modulus Implant," *PLoS One*, 2013.
- [40] A. P. Md Saad, A. T. Prakoso, M. A. Sulong, H. Basri, D. A. Wahjuningrum, and A. Syahrom, "Impacts of dynamic degradation on the morphological and mechanical characterisation of porous magnesium scaffold," *Biomech. Model. Mechanobiol.*, 2019.
- [41] A. P. Md Saad *et al.*, "The influence of flow rates on the dynamic degradation behaviour of porous magnesium under a simulated environment of human cancellous bone," *Mater. Des.*, vol. 122, pp. 268–279, 2017.
- [42] A. Syahrom, M. R. Abdul Kadir, J. Abdullah, and A. Öchsner, "Mechanical and microarchitectural analyses of cancellous bone through experiment and computer simulation," *Med. Biol. Eng. Comput.*, vol. 49, no. 12, pp. 1393–1403, 2011.